Distributed Optimal Control of Sensor Networks for Dynamic Target Tracking

Greg Foderaro, *Member, IEEE*, Pingping Zhu, *Member, IEEE*, Hongchuan Wei, Thomas A. Wettergren, *Senior Member, IEEE*, and Silvia Ferrari, *Senior Member, IEEE*

***Abstract*—This paper presents a distributed optimal control approach for managing omnidirectional sensor networks deployed to cooperatively track moving targets in a region of interest. Several authors have shown that under proper assumptions, the performance of mobile sensors is a function of the sensor distribution. In particular, the probability of cooperative track detection, also known as track coverage, can be shown to be an integral function of a probability density function representing the macroscopic sensor network state. Thus, a mobile sensor network deployed to detect moving targets can be viewed as a multiscale dynamical system in which a time-varying probability density function can be identified as a restriction operator, and optimized subject to macroscopic dynamics represented by the advection equation. Simulation results show that the distributed control approach is capable of planning the motion of hundreds of cooperative sensors, such that their effectiveness is significantly increased compared to that of existing uniform, grid, random, and stochastic gradient methods.**

***Index Terms*—Distributed control, mobile sensor networks, multiscale dynamical systems, optimal control, target tracking, track coverage.**

I. Introduction

THIS paper presents a distributed optimal control (DOC) approach for optimizing the trajectories of a network of many cooperative mobile sensors deployed to perform track detection in a region of interest (ROI). Considerable attention has been given to the problem of controlling mobile sensors in order to maximize coverage in a desired ROI, as required when no prior target information is available [1]–[9]. When prior information, such as target measurements or expert knowledge, is available, optimal control and information-driven strategies have been shown to significantly outperform other methods [8]–[15]. Due to the computational complexity associated with solving the optimality conditions and evaluating information theoretic functions, however, these methods typically do not scale to networks with hundreds of sensors because the computation they require increases exponentially with the number of agents [16].

Distributed optimal control has been recently shown to overcome the computational complexity associated with classical optimal control for systems in which the network performance or cost function is a function of a suitable restriction operator, such as a probability density function (PDF) or maximum-likelihood estimator (MLE) [17]–[20]. Several authors have shown that, in many instances, the performance of networks of cooperative agents, such as sensors and robotic vehicles, is a function of a PDF representing the density of the agents over the ROI [21]–[25]. Thus, one approach that has been proposed to deploy many cooperative agents is to sample a known PDF to obtain a set of agent positions in the ROI [25]. Another approach is to use a known PDF to perform locational optimization, and obtain a corresponding network representation using centroidal Voronoi partitions [26], [27]. Alternatively, agent trajectories can be computed using a hierarchical control approach that first establishes a virtual, adaptive network boundary, and then computes the agent control inputs to satisfy the boundary in a lower-dimensional space [28].

While these existing approaches are effective at reducing the dimensionality of an otherwise intractable optimal control problem, they assume that the optimal PDF (or virtual boundary) are given *a priori*. As a result, the agents may be unable to reach the desired PDF when in the presence of dynamic constraints and/or inequality constraints on the state and controls. Conversely, if a conservative PDF is given to guarantee reachability, network performance may be suboptimal. Furthermore, because existing methods assume stationary agent distributions, they cannot fully exploit the capabilities of mobile sensors, or take into account time-varying environmental conditions. The DOC approach, recently developed by the authors in [18], overcomes these limitations by optimizing a time-varying agent PDF subject to the agent dynamics.

To date, DOC optimality conditions have been derived and used to solve network control problems in multi-agent path planning and navigation [18], [20]. This paper presents conservation law results that show the closed-loop DOC system is Hamiltonian. Based on these results, an efficient numerical solution is obtained using a finite volume discretization scheme that has a computational complexity far reduced compared to classical optimal control. The DOC method is then applied to a network control problem in which omnidirectional sensors are deployed to cooperatively detect moving targets in an obstacle-populated ROI. Several authors have shown that the tracking

Manuscript received November 14, 2015; revised May 4, 2016; accepted June 6, 2016. Date of publication June 21, 2016; date of current version March 16, 2018. This work was supported by the ONR Code 321. Recommended by Associate Editor Y. Zhang.

G. Foderaro and H. Wei are with the Department of Mechanical Engineering and Materials Science, Duke University, Durham, NC 27708, USA (e-mail: greg.foderaro@duke.edu; hongchuan.wei@duke.edu).

P. Zhu and S. Ferrari are with the Sibley School of Mechanical and Aerospace Engineering, Cornell University, Ithaca, NY 14853, USA (e-mail: pingping.zhu@cornell.edu; ferrari@cornell.edu).

T. A. Wettergren is with the Naval Undersea Warfare Center, Newport, RI 02841, USA (e-mail: t.a.wettergren@ieee.org).

Color versions of one or more of the figures in this paper are available online at http://ieeexplore.ieee.org.

Digital Object Identifier 10.1109/TCNS.2016.2583070

and detection capability of many real sensor networks, such as passive acoustic sensors, can be represented in closed-form by assuming the sensors are omnidirectional and prior targets measurements can be assimilated into Markov motion models (see [9], [10], [29]–[32] and references therein). In this paper, the DOC approach is used to optimize the detection capability of this class of sensor networks for hundreds of cooperative agents. In particular, the optimal DOC control laws optimize a weighted tradeoff of multiple conflicting objectives, namely, probability of detection, energy consumption, and collision avoidance. The results show that the DOC approach significantly improves the probability of detection compared to other scalable strategies known as uniform, grid, along with random and stochastic gradient methods [33], [34].

II. Problem Formulation and Assumptions

This paper considers the problem of optimizing the state and control trajectories of a network of N mobile sensors used to detect a moving target in an obstacle-populated ROI $\mathcal{A} = [0, L] \times [0, L] \subset \mathbb{R}^2$ during a fixed time interval $t \in (T_0, T_f]$, where T_0 and T_f are both given. Each sensor is mounted on a robot or vehicle whose motion is governed by a small system of ODEs

$$\dot{\mathbf{s}}_i(t) = \mathbf{f}\left[\mathbf{s}_i(t), \mathbf{u}_i(t), t\right], \quad \mathbf{s}_i(T_0) = \mathbf{s}_{i_0}, \quad i = 1, \ldots, N \tag{1}$$

where $\mathbf{s}_i(t) = [\mathbf{x}_i^T(t) \quad \theta_i(t)]^T \in \mathcal{S}$ is the ith vehicle state comprised of the vehicle position $\mathbf{x}_i = [x_i \quad y_i]^T \in \mathcal{A}$ and heading angle $\theta_i \in [0, 2\pi)$, $\mathbf{u}_i \in \mathcal{U} \subset \mathbb{R}^m$ is the vehicle control vector, and $\mathcal{U}$ is the space of m-admissible control inputs. Here, the superscript "T" denotes the transpose of matrices and vectors. Each sensor is assumed to be omnidirectional, with a constant effective range $r \in \mathbb{R}$, defined as the maximum range at which the received signal exceeds a desired threshold [8]. Then, the field of view (FOV) of every sensor can be modeled by a disk $\mathcal{C}(\mathbf{x}_i, r) \subset \mathbb{R}^2$, with radius r and center at $\mathbf{x}_i$.

Since $\mathbf{x}_i$, $i = 1, \ldots, N$, is a time-varying continuous vector, let $\wp_{\mathbf{x}_i}$ denote the time-varying PDF of $\mathbf{x}_i$, defined as a nonnegative function that satisfies the normalization property

$$\int_{\mathcal{A}} \wp_{\mathbf{x}_i}(\mathbf{x}_i, t) d\mathbf{x}_i = 1 \tag{2}$$

and such that the probability of event $\mathbf{x}_i \in \mathcal{B} \subset \mathcal{A}$ is

$$P(\mathbf{x}_i \in \mathcal{B}, t) = \int_{\mathcal{B}} \wp_{\mathbf{x}_i}(\mathbf{x}_i, t) d\mathbf{x}_i \tag{3}$$

where $\mathcal{B}$ is any subset of the ROI, and, for brevity, $\wp_{\mathbf{x}_i}$ is abbreviated to $\wp$ in the remainder of this paper. With this approach, each sensor can be viewed as a fluid particle in the Lagrangian approach, and $\wp$ can be viewed as the forward PDF of particle position [35]. Therefore, $N\wp$ represents the density of sensors in $\mathcal{A}$.

There is considerable precedence in both target tracking literature and practice for modeling target dynamics by Markov motion models that assimilate multiple, distributed sensor measurements [36], [37]. These tracking algorithms have the ability to incrementally update the target model over time and output Markov transition probability density functions (PDFs) that describe the uncertainty associated with the target based on prior sensor measurements. This paper shows that the target PDFs obtained by the tracking algorithms can be used as feedback to a distributed optimal control algorithm, such that the sensor motion can be planned in order to maximize the expected number of target detections over a desired time interval. Subsequently, the target PDFs can be updated to reflect the new knowledge obtained by the sensor network controlled via DOC.

Let the target (T) motion be described by the unicycle kinematic equations

$$\dot{\mathbf{x}}_T(t) = \begin{bmatrix} \dot{x}_T(t) \\ \dot{y}_T(t) \end{bmatrix} = \begin{bmatrix} v_T(t)\cos\theta_T(t) \\ v_T(t)\sin\theta_T(t) \end{bmatrix}, \ t \in (T_0, T_f] \tag{4}$$

where $\mathbf{x}_T(t) = [x_T(t), y_T(t)]^T \in \mathcal{A}$ is the target state, $v_T(t)$ is the target velocity, and $\theta_T(t)$ is the target heading angle. Because many vehicles and targets of interest move at constant heading over some period of time, Markov motion models assume that the target heading and velocity are constant during a sequence of time subintervals $(t_j, t_{j+1}] \subset (T_0, T_f]$, $j = 1, \ldots, m$, that together comprise an exact cover of $(T_0, T_f]$. At any time t_j, $j = 1, \ldots, m$, the target may change both heading and velocity and thus t_j is also referred to as maneuvering time. Then, introducing the discrete-time variables $\mathbf{x}_{T_j} = \mathbf{x}_T(t_j)$, $\theta_{T_j} = \theta_T(t_j)$, and $v_{T_j} = v_T(t_j)$, and integrating (4) with respect to time, the target can be described by the motion model

$$\mathbf{x}_{T_{j+1}} = \mathbf{x}_{T_j} + \left[v_{T_j}\cos\theta_{T_j} \quad v_{T_j}\sin\theta_{T_j}\right]^T \Delta t_j \tag{5}$$

where $\Delta t_j = t_{j+1} - t_j$and $j = 1, \ldots, m$.

Because the actual target track is unknown *a priori*, $\mathbf{x}_{T_j}$, θ_{T_j}, and $\mathbf{v}_{T_j}$ can be viewed as random variables [36], [37]. Assuming for simplicity that they are independent random variables, prior target information can be provided in terms of the target PDFs $f\mathbf{x}_{T_j}(\mathbf{x}_{T_j})$, $f_{\Theta_{T_j}}(\theta_{T_j})$, and $f_{V_{T_j}}(v_{T_j})$that may computed by target tracking algorithms based on prior sensor measurements [38] or are otherwise assumed uniform.

For an omnidirectional sensor, the probability of target detection for a sensor at $\mathbf{x}_i$ can be described by the Boolean detection model

$$P_s\left[\mathbf{x}_i(t), \mathbf{x}_T(t)\right] = \begin{cases} 1, & \|\mathbf{x}_i(t) - \mathbf{x}_T(t)\| \leq r \\ 0, & \|\mathbf{x}_i(t) - \mathbf{x}_T(t)\| > r, \end{cases} \tag{6}$$

where $\|\cdot\|$ denotes the Euclidean norm [25], [30].

The problem considered in this paper is to optimally control the N omnidirectional sensors such that the weighted tradeoff of multiple conflicting objectives, namely, probability of track detection, energy consumption, and collision avoidance in $\mathcal{A}$ is optimized subject to the equation of motion (1). The next section shows how this problem can be formulated as a DOC problem and, then, solved efficiently for up to hundreds of

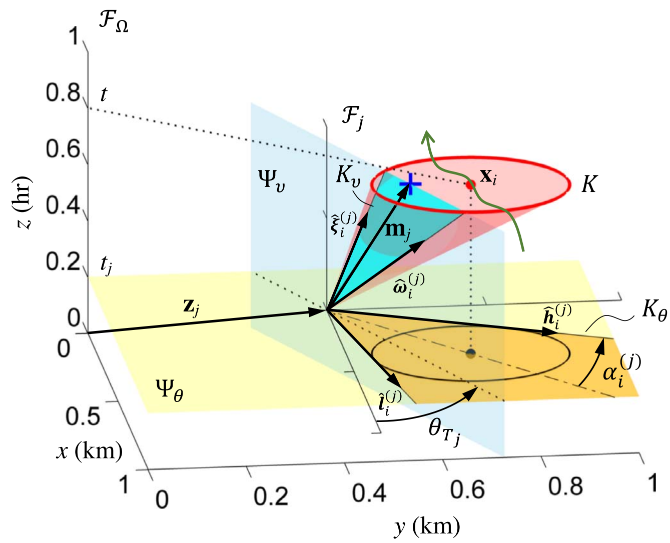

Fig. 1. Example of 3-D coverage cone $K(t)$ (magenta), and corresponding 2-D representation comprised of the pair of heading-cone K_θ (orange) and velocity-cone K_v (cyan).

sensors using the conservation law analysis and numerical method presented in Sections V and VI.

III. Probability of Target Detection

The quality-of-service of a sensor network deployed to detect and track a moving target in an ROI $\mathcal{A}$ can be represented in closed form by a track coverage function derived using geometric transversals [10]. The track coverage function represents the probability of detecting a target on a track in a spatiotemporal space, defined as $\Omega = \mathcal{A} \times (T_0, T_f]$. Let $\mathcal{F}_\Omega$ denote an inertial frame embedded in Ω and, for every time interval $(t_j, t_{j+1}]$, consider a local frame of reference $\mathcal{F}_j$ with an origin at $\mathbf{z}_j = [\mathbf{x}_{T_j}^T \;\; t_j]^T \in \Omega$, as shown in Fig. 1. Then, based on the Markov motion model in Section II, the target track as it evolves from time t_j to any time t, $t \in (t_j, t_{j+1}]$, can be represented by a time-varying vector $\mathbf{m}_j(t)$ in $\mathcal{F}_j$, defined as $\mathbf{m}_j(t) = [\mathbf{x}_T(t)^T \quad t]^T - \mathbf{z}_j$ Fig. 1. From the sensor model in (6), the ith sensor is able to detect the target at time t if and only if $\|\mathbf{x}_T(t) - \mathbf{x}_i(t)\| \leq r$. Thus, the set of all target tracks detected is contained by a time-varying 3-D coverage cone defined according to the following remark, proven in [10]:

Remark 3.1: The coverage cone defined as

$$K(t) = \Big\{ [x \;\; y \;\; z]^T \in \Omega \subset \mathbb{R}^3 \big| z > t_j, t \in (t_j, t_{j+1}]$$

$$\times \left\| [x \quad y]^T - \frac{(z-t_j)}{(t-t_j)} [\mathbf{x}_i(t) - \mathbf{x}_{T_j}] - \mathbf{x}_{T_j} \right\| \leq \frac{(z-t_j)}{(t-t_j)} r \Big\} \tag{7}$$

contains the set of all target tracks that intersect the ith sensor's FOV $\mathcal{C}(t)$at any time $t \in (t_j, t_{j+1}]$.

An example of coverage cone is shown in Fig. 1, where $K(t)$ (magenta) is plotted at time $t = 0.8$ (hr), for a sensor that moves along a trajectory $\mathbf{x}_i(t)$ (green line) and has the FOV shown by a red disk. Because (7) is a circular cone that is possibly oblique, it is difficult to define a Lebesgue measure of the tracks contained by $K(t)$ that can be computed analytically from the sensor position and the Markov parameters. By extending the approach in [10] to a moving sensor, $K(t)$ can be represented by a pair of 2-D cones, referred to as *heading cone* and *velocity cone*, for which a Lebesgue measure of the tracks detected by a sensor at $\mathbf{x}_i(t)$ can be provided in terms of unit vectors. The 2-D representation of the coverage cone in Fig. 1 is plotted in orange (heading cone) and cyan (velocity cone), and derived in the remainder of this subsection.

Let the 2-D heading cone K_θ be defined as the projection of K onto the plane

$$\Psi_\theta = \left\{ [x \;\; y \;\; z]^T \in \Omega \mid z = t_j \right\}. \tag{8}$$

such that K_θ (shown in yellow in Fig. 1) contains all possible headings of a target detected by the ith sensor at any time $t \in (t_j, t_{j+1}]$. Since K_θ is a 2-D cone, it can be expressed as a linear combination of two unit vectors on the heading plane with respect to a local coordinate frame $\mathcal{F}_j$ such that

$$K_\theta [\mathbf{x}_i(t), \mathbf{z}_j] = \left\{ c_1 \hat{\boldsymbol{h}}_i^{(j)}(t) + c_2 \hat{\boldsymbol{l}}_i^{(j)}(t) \big| c_1, c_2 \geq 0 \right\}, \tag{9}$$

where

$$\hat{\mathbf{h}}_i^{(j)}(t) = \begin{bmatrix} \cos\alpha_i^{(j)}(t) & -\sin\alpha_i^{(j)}(t) \\ \sin\alpha_i^{(j)}(t) & \cos\alpha_i^{(j)}(t) \\ 0 & 0 \end{bmatrix} \frac{\mathbf{d}^{(j)}(t)}{\|\mathbf{d}^{(j)}(t)\|}$$

$$\equiv \begin{bmatrix} \cos\lambda_i^{(j)}(t) \\ \sin\lambda_i^{(j)}(t) \\ 0 \end{bmatrix}, \tag{10}$$

$$\hat{\mathbf{l}}_i^{(j)}(t) = \begin{bmatrix} \cos\alpha_i^{(j)}(t) & \sin\alpha_i^{(j)}(t) \\ -\sin\alpha_i^{(j)}(t) & \cos\alpha_i^{(j)}(t) \\ 0 & 0 \end{bmatrix} \frac{\mathbf{d}_i^{(j)}(t)}{\left\|\mathbf{d}_i^{(j)}(t)\right\|}$$

$$\equiv \begin{bmatrix} \cos\gamma_i^{(j)}(t) \\ \sin\gamma_i^{(j)}(t) \\ 0 \end{bmatrix}$$

$\mathbf{d}_i^{(j)}(t) \triangleq (\mathbf{x}_i(t) - \mathbf{x}_{T_j})$ and $\alpha_i^{(j)}(t) = \sin^{-1}(r/\|\mathbf{d}_i^{(j)}(t)\|)$.

Now, let the velocity cone K_v be defined as the intersection of K with the velocity plane

$$\Psi_v = \{[x \;\; y \;\; z]^T \in \Omega \mid (x \sin\theta_{T_j} - y\cos\theta_{T_j})$$

$$= [\sin\theta_{T_j} \cos\theta_{T_j}]\mathbf{x}_{T_j}, \quad z \geq t_j\}.$$

such that K_v represents the speeds of all targets with heading θ_{T_j} (contained in K_θ) that are detected by the ith sensor at $t \in (t_j, t_{j+1}]$. The velocity cone K_v can be represented by two unit vectors defined with respect to $\mathcal{F}_j$ such that

$$K_v [\mathbf{x}_i(t), \mathbf{z}_j] = \left\{ c_1 \hat{\boldsymbol{\xi}}_i^{(j)}(t) + c_2 \hat{\boldsymbol{\omega}}_i^{(j)}(t) \big| c_1, c_2 \geq 0 \right\} \tag{11}$$

where

$$\hat{\boldsymbol{\xi}}_i^{(j)}(t) = \begin{bmatrix} \sin\eta_i^{(j)}(t)\cos\theta_{T_j} \\ \sin\eta_i^{(j)}(t)\sin\theta_{T_j} \\ \cos\eta_i^{(j)}(t) \end{bmatrix},$$

$$\hat{\boldsymbol{\omega}}_i^{(j)}(t) = \begin{bmatrix} \sin\mu_i^{(j)}(t)\cos\theta_{T_j} \\ \sin\mu_i^{(j)}(t)\sin\theta_{T_j} \\ \cos\mu_i^{(j)}(t) \end{bmatrix},$$

$$\eta_i^{(j)}(t) = \tan^{-1}\left[\frac{1}{t-t_j}\left(\left[\cos\theta_{T_j}\ \sin\theta_{T_j}\right]\left[\mathbf{x}_i(t)-\mathbf{x}_{T_j}\right] - \sqrt{r^2-\left(\left[\sin\theta_{T_j}\ -\cos\theta_{T_j}\right]\left[\mathbf{x}_i(t)-\mathbf{x}_{T_j}\right]\right)^2}\right)\right],$$

$$\mu_i^{(j)}(t) = \tan^{-1}\left[\frac{1}{t-t_j}\left(\left[\cos\theta_{T_j}\ \sin\theta_{T_j}\right]\left[\mathbf{x}_i(t)-\mathbf{x}_{T_j}\right] + \sqrt{r^2-\left(\left[\sin\theta_{T_j}\ -\cos\theta_{T_j}\right]\left[\mathbf{x}_i(t)-\mathbf{x}_{T_j}\right]\right)^2}\right)\right]. \tag{12}$$

An example of these coverage cone representations is illustrated in Fig. 1.

As proven in [10], the pair of 2-D time-varying cones $\{K_\theta, K_v\}$ can be used to represent all tracks contained by the 3-D time-varying coverage cone K. It follows that the probability of detection by the ith sensor at time $t \in (t_j, t_{j+1}]$ is the probability that the Markov parameters are contained by the heading and velocity cones, i.e.,

$$P_d(t) \equiv P\left[\mathbf{m}_j(t) \in K(t)\right] = \int_{\mathcal{A}} f_{\mathbf{X}_{T_j}}(\mathbf{x}_{T_j}) \int_{\gamma_i^{(j)}(t)}^{\lambda_i^{(j)}(t)} f_{\Theta_{T_j}}(\theta_{T_j}) \times \int_{\tan\eta_i^{(j)}(t)}^{\tan\mu_i^{(j)}(t)} f_{V_{T_j}}(v_{T_j})\, dv_{T_j}\, d\theta_{T_j}\, d\mathbf{x}_{T_j} \tag{13}$$

where the Markov motion PDFs are known from the tracking algorithms (Section II).

IV. Distributed Optimal Control Problem

The control of the N omnidirectional sensors is achieved by optimizing a weighted sum of the probability of target detection, energy consumption, and collision avoidance in the ROI. The energy consumption can be modeled as a quadratic function of the vehicle-control vector $\mathbf{u}_i$. By introducing a repulsive potential function U_{rep} generated from the obstacle geometries [18], [39], the obstacle avoidance objective can be expressed as the product of $\wp$ and U_{rep}. Then, the total sensor network performance can expressed as the integral cost function

$$J = \sum_{j=1}^{m}\int_{t_j}^{t_{j+1}}\int_{\mathcal{A}}\left[w_r\wp(\mathbf{x}_i,t)U_{rep} - w_d\wp(\mathbf{x}_i,t)P_d(t) + w_e\mathbf{u}_i^T\mathbf{R}\mathbf{u}_i\right]d\mathbf{x}_i dt \triangleq \sum_{j=1}^{m}\int_{t_j}^{t_{j+1}}\int_{\mathcal{A}}\mathscr{L}\{\wp(\mathbf{x}_i,t),\mathbf{u}_i,t\}d\mathbf{x}_i dt \tag{14}$$

and must be minimized with respect to the network state $\wp$ and control law $\mathbf{u}_i = \mathbf{c}[\wp(\mathbf{x}_i,t)]$subject to (1),(2), (3). The constant weights w_d, w_r, and w_e, are chosen by the user based on the desired tradeoff between the sensing, obstacle-avoidance, and energy objectives, and $\mathbf{R}$ is a diagonal positive-definite matrix.

Because the dynamic constraints (1) are a function of the sensor (microscopic) state and control, $\mathbf{x}_i$ and $\mathbf{u}_i$, the next step is to determine the macroscopic evolution of $\wp$ subject to (1). It was shown in [18] and [20] that if agents are never created nor destroyed and are advected by a known velocity field (1), then the evolution of $\wp$ can be described by the advection equation. The advection equation is a hyperbolic partial differential equation (PDE) that governs the motion of a conserved, scalar quantity, such as a PDF, when subject to a known velocity field [40]. From (1), the PDF $\wp$ is advected by the velocity field $\mathbf{v}_i = \dot{\mathbf{x}}_i$, resulting in macroscopic dynamics

$$\frac{\partial\wp}{\partial t} = -\nabla\cdot\{\wp(\mathbf{x}_i,t)\mathbf{v}_i\} = -\nabla\cdot\{\wp(\mathbf{x}_i,t)\mathbf{f}[\mathbf{s}_i,\mathbf{u}_i,t]\}. \tag{15}$$

The gradient ∇ represents a row vector of partial derivatives with respect to $\mathbf{x}_i$, and $(\cdot)$ denotes the dot product.

Because the initial agent distribution is usually given, based on the initial positions of the sensors in the ROI, the PDE (15) is subject to the initial condition

$$\wp[\mathbf{x}_i, T_0] = \wp_0(\mathbf{x}_i). \tag{16}$$

Also, in order to guarantee that agents are neither created nor destroyed in $\mathcal{A}$, the PDE (15) is subject to the boundary condition

$$\wp[\mathbf{x}_i \in \partial\mathcal{A}, t] = 0, \ \ \forall t \in (T_0, T_f] \tag{17}$$

state constraints

$$\wp[\mathbf{x}_i \notin \mathcal{A}, t] = 0, \ \ \forall t \in (T_0, T_f] \tag{18}$$

and the normalization condition (2).

Now, consider a square area $\mathcal{A}' \subset \mathcal{A}$ with side length Δx. In order to guarantee independent detections, the density of the sensors in the area $\mathcal{A}'$ must satisfy the following inequality:

$$\frac{(\Delta x)^2}{\pi r^2} \geq N(\Delta x)^2\wp(\mathbf{x}_i', t), \quad \mathbf{x}_i' \in \mathcal{A}' \tag{19}$$

where $\wp(\cdot)$ can be assumed constant in $\mathcal{A}'$ for a small Δx. The right-hand side (RHS) in (19) is the number of the sensors in the area $\mathcal{A}$, and the left-hand side (LHS) in (19) is a upper bound. Then, the following constraint can be obtained:

$$\wp(\mathbf{x}_i, t) \leq \frac{1}{N\pi r^2} \tag{20}$$

and is used to guarantee that there are no overlapping FOVs or, in other words, that sensor detections are independent. The analysis presented in the next section shows that the closed-loop DOC problem is a Hamiltonian system and, thus, the agent PDF $\wp$ is conserved over time. As a result, numerical solutions of the DOC problem can be obtained using conservative numerical algorithms, such as finite volume (FV), that are known to be computationally efficient and allow for coarse-grain discretizations without dissipation errors [41].

V. Conservation Law Analysis

Hamiltonian systems are characterized by a constant of motion, or Hamiltonian function, by which optimal trajectories can be shown to have vanishing variations along this constant of motion, according to Pontryagin's minimum principle [42], [43]. Because in the DOC problem, the coarse dynamics are described by the advection equation (15), the open-loop system is inherently conservative [44]. The goal of this section is to show that the controlled dynamics (or closed-loop system) is also conservative, by proving that it satisfies Hamilton equations

$$\frac{\partial \psi}{\partial \mathbf{q}} = -\frac{d\mathbf{p}}{dt}, \ \frac{\partial \psi}{\partial \mathbf{p}} = \frac{d\mathbf{q}}{dt} \tag{21}$$

where $\psi = \psi(\mathbf{p}, \mathbf{q}, t)$ is the Hamiltonian function, $\mathbf{q} = \mathbf{q}(t) \in \mathbb{R}^n$ are the generalized coordinates, and $\mathbf{p} = \mathbf{p}(t) \in \mathbb{R}^n$ are the generalized momenta.

For simplicity, the proof is presented for $n = 2$, where $\mathbf{x}_i = [x_i \quad y_i]^T$ denotes the position of the ith agent in $\mathbb{R}^2$. Then, the Hamiltonian function is determined by recasting the detailed equation (1) into a 3-D time-invariant ODE. Letting $\hat{\mathbf{x}}_i = [\mathbf{x}_i^T t]^T$ and $\hat{\mathbf{u}}_i = \mathbf{c}[\wp(\mathbf{x}_i, t)] = \mathbf{c}[\wp(\hat{\mathbf{x}}_i)]$, the sensor equation of motion (1) can be written as

$$\dot{\hat{x}}_i(t) = [\dot{x}_i(\hat{\mathbf{x}}_i, \hat{\mathbf{u}}_i) \quad \dot{y}_i(\hat{\mathbf{x}}_i, \hat{\mathbf{u}}_i) \quad 1]^T = \hat{\mathbf{f}}(\hat{\mathbf{x}}_i, \hat{\mathbf{u}}_i) \tag{22}$$

in the time-space domain Ω. It also follows that the macroscopic evolution equation (15) can be rewritten as

$$\frac{\partial \wp(\hat{\mathbf{x}}_i)}{\partial t} + \frac{\partial \left[\wp(\hat{\mathbf{x}}_i)\dot{x}_i(\hat{\mathbf{x}}_i, \hat{\mathbf{u}}_i)\right]}{\partial x_i} + \frac{\partial \left[\wp(\hat{\mathbf{x}}_i)\dot{y}_i(\hat{\mathbf{x}}_i, \hat{\mathbf{u}}_i)\right]}{\partial y_i} = 0 \tag{23}$$

where, now $\wp$ is only a function of $\hat{\mathbf{x}}_i$.

Now, let $\mathbf{A} \equiv [A_x \ \ A_y \ \ A_t] = \mathbf{A}(\hat{\mathbf{x}}_i)$ denote the vector potential of the product $(\wp\hat{\mathbf{u}}_i)$ i.e.,

$$\wp(\hat{\mathbf{x}}_i)\hat{\mathbf{u}}_i(\hat{\mathbf{x}}_i) = \nabla \times \mathbf{A}(\hat{\mathbf{x}}_i). \tag{24}$$

By performing a coordinate transformation to a canonical reference frame defined such that $A_y = 0$, $\mathbf{A}$ can be used to relate the 2-D time-varying system to the 3-D time-invariant form, such that the Hamiltonian functions for the two forms are equivalent [44], [45]. The coordinate transformation is then given by $\mathcal{F} : \hat{\mathbf{x}}_i \rightarrow \tilde{\mathbf{x}}_i$, where $\tilde{\mathbf{x}}_i = [x_i \ a \ t]^T$ and

$$a = -A_x[x_i, h(x_i, a, t), t]. \tag{25}$$

The resulting vector potential is

$$\mathbf{A} = \left[A_x(x_i, h(x_i, a, t), t) \quad 0 \quad A_t(x_i, h(x_i, a, t), t)\right],$$

which is governed by

$$\wp \, \dot{x}_i = \frac{\partial A_t}{\partial y_i}, \ \wp \, \dot{y}_i = \frac{\partial A_x}{\partial t} - \frac{\partial A_t}{\partial x_i}, \ \wp = -\frac{\partial A_x}{\partial y_i} \tag{26}$$

where the function $h(x_i, a, t)$ is implicitly defined in (25). Then, the equivalent system is

$$\frac{d\tilde{\mathbf{x}}_i}{dt} = \tilde{\mathbf{f}}(\tilde{\mathbf{x}}_i) = \begin{bmatrix} \frac{\partial A_t}{\partial a} & -\frac{\partial A_t}{\partial x_i} & 1 \end{bmatrix}^T \tag{27}$$

and the time scales in the physical and canonical forms are also equivalent.

Finally, choose the Hamiltonian function

$$\psi(x_i, a, t) = A_t[x_i, h(x_i, a, t), t]. \tag{28}$$

By substituting (28) into (27), Hamilton equations in (21) are satisfied as follows:

$$\frac{\partial \psi}{\partial x_i} = -\frac{da}{dt}, \quad \frac{\partial \psi}{\partial a} = \frac{dx_i}{dt} \tag{29}$$

and are equivalent to a 2-D time-varying system in canonical space $\tilde{\Omega} = \mathcal{F}(\Omega)$, with Hamiltonian function ψ. Furthermore, this Hamiltonian formulation holds for any system governed by (1) and (15), and is mathematically equivalent to the Lagrangian fluid transport for unsteady flow in two dimensions [44], proving the conservation law for (15).

VI. Numerical Solution of DOC Problem

The necessary conditions for optimality conditions for the DOC problems in the form of (14)–(18) were recently derived in [18]. These optimality conditions amount to a set of parabolic PDEs without a known analytical solution. This section presents a direct DOC solution method that parameterizes the agent PDF by a finite Gaussian mixture model, and discretizes the continuous DOC problem about a finite set of collocation points to obtain a nonlinear program (NLP) that is solved numerically using sequential quadratic programming (SQP). Based on the conservation analysis results in Section V, the discretized DOC problem can be obtained using an efficient FV discretization scheme that has a computational complexity far reduced compared to classical optimal control.

It is assumed that the optimal sensor PDF can be approximated by a finite Gaussian mixture model (GMM) [46] obtained from the linear superposition of Z time-varying components with density

$$f_j(\mathbf{x}_i, t) = \frac{1}{(2\pi)^{\frac{n}{2}}|\mathbf{\Sigma}_j|^{\frac{1}{2}}} e^{\left[-\left(\frac{1}{2}\right)(\mathbf{x}_i - \boldsymbol{\mu}_j)^T \Sigma_j^{-1}(\mathbf{x}_i - \boldsymbol{\mu}_j)\right]} \tag{30}$$

where $j = 1, \ldots, Z$, $|\cdot|$ denotes the matrix determinant, $(\cdot)^{-1}$ denotes the matrix inverse, $\boldsymbol{\mu}_j \in \mathbb{R}^n$ is a time-varying mean vector, $\boldsymbol{\Sigma}_j \in \mathbb{R}^{n \times n}$ is a time-varying covariance matrix, and Z is an integer chosen by the user. Thus, at any time $t \in (T_0, T_f]$ the optimal agent distribution can be represented as

$$\wp(\mathbf{x}_i, t) = \sum_{j=1}^{Z} w_j(t) f_j(\mathbf{x}_i, t) \tag{31}$$

where the mixing proportions or weights $w_1, \ldots, w_Z$ obey $0 \leq w_j \leq 1\ \forall j$ and $\sum_{j=1}^{Z} w_j = 1$ at all times [33].

An approximately optimal agent distribution $\wp^*$ can be obtained by determining the optimal trajectories of the mixture model parameters w_j, $\boldsymbol{\mu}_j$, and $\boldsymbol{\Sigma}_j$, for $j = 1, \ldots, Z$. Let Δt denote a constant discretization time interval, and k denote a discrete time index, such that $\Delta t = (T_f - T_0)/K$ and thus $t_k = k\Delta t$, for $k = 0, \ldots, K$. Assume that the microscopic control inputs $\mathbf{u}$ are piecewise constant during every time interval Δt and that

$$\begin{aligned}\wp_k &\triangleq \wp(\mathbf{x}_i, t_k) \approx \sum_{j=1}^{Z} w_j(t_k) f_j(\mathbf{x}_i, t_k) \\ &\equiv \sum_{j=1}^{Z} w_{jk} \frac{1}{(2\pi)^{\frac{n}{2}} |\boldsymbol{\Sigma}_{jk}|^{\frac{1}{2}}} e^{\left[-\left(\frac{1}{2}\right)(\mathbf{x}_i - \boldsymbol{\mu}_{jk})^T \Sigma_{jk}^{-1} (\mathbf{x}_i - \boldsymbol{\mu}_{jk})\right]}\end{aligned} \tag{32}$$

represents the agent distribution at t_k. Then, the weights w_{jk} and the elements of $\boldsymbol{\mu}_{jk}$ and $\boldsymbol{\Sigma}_{jk}$, for all j and k are organized into a vector $\boldsymbol{\zeta}$ of parameters to be determined such that the DOC cost function (14) is minimized, the DOC constraints (15)–(18) are satisfied, and such that the component densities $f_1, \ldots, f_L$ are non-negative and obey the normalization condition for all k.

Since $\wp$ is a conserved quantity of a Hamiltonian system (Section V), the evolution equation (15) can be discretized using a conservative FV discretization algorithm that does not suffer from dissipative error when using a coarse-grained state discretization [41]. The FV algorithm adopted in this paper partitions the state space $\mathcal{A}$ into finite volumes defined by a constant discretization interval $\Delta \mathbf{x} \in \mathbb{R}^n$ that are each centered about a collocation point $\mathbf{x}_l \in \mathcal{A} \subset \mathbb{R}^n$, $l = 1, \ldots, X$.

Now, let $\wp_{l,k}$ and $\mathbf{u}_{l,k}$ denote FV approximations of $\wp(\mathbf{x}_l, t_k)$ and $\mathbf{c}[\wp(\mathbf{x}_l, t_k)]$, respectively. Then, the FV approximation of the evolution equation (15) is obtained by applying the divergence theorem to (15) in every finite volume, such that $\wp_{k+1} = \wp_k + \Delta t \rho_k$, where

$$\rho_k \triangleq -\int_S [\wp_k \mathbf{f}(\mathbf{s}_{l,k}, \mathbf{u}_{l,k}, t_k)] \cdot \hat{\mathbf{n}}\, dS \tag{33}$$

and S and $\hat{\mathbf{n}}$ denote the finite volume boundary and unit normal, respectively. To ensure numerical stability, the discretization intervals Δt and $\Delta \mathbf{x}$ are chosen to satisfy the Courant-Friedrichs-Lewy condition [41].

Then, letting $\Delta \mathbf{x}_{(j)}$ denote the jth element of $\Delta \mathbf{x}$, the discretized DOC problem can be written as the finite-dimensional NLP

$$\begin{aligned}&\min\ J_D = \sum_{j=1}^{n} \Delta \mathbf{x}_{(j)} \sum_{l=1}^{X} \left[\phi_{l,K} + \Delta t \sum_{k=1}^{K} \mathscr{L}(\wp_{l,k}, \mathbf{u}_{l,k}, t_k)\right] \\ &\text{sbj to } \wp_{k+1} - \wp_k - \Delta t \rho_k = 0,\ k = 1, \ldots, K \\ &\sum_{j=1}^{n} \Delta \mathbf{x}_{(j)} \sum_{l=1}^{X} \wp_{l,k} - 1 = 0,\ k = 1, \ldots, K \\ &\wp_{l,0} = g_0(\mathbf{x}_l),\ \forall \mathbf{x}_l \in \mathcal{A} \\ &\wp_{l,k} = 0,\ \forall \mathbf{x}_l \in \partial\mathcal{A},\ k = 1, \ldots, K \\ &\wp_k \leq \frac{\Delta \mathbf{x}_{(j)}}{N\pi r^2}\ k = 1, \ldots, K\end{aligned} \tag{34}$$

where $\wp_{l,0}$ is the initial distribution at $\mathbf{x}_l$, and $\phi_{l,K} \triangleq \phi(\wp_{l,K})$ is the terminal constraint. In addition, the inequality results from the geometric constraint in (20).

From (32), it can be seen that $\wp_{l,k}$ and $\mathbf{u}_{l,k}$ are functions solely of the mixture model parameters $\boldsymbol{\zeta}$ and, thus, the elements of $\boldsymbol{\zeta}$ constitute the NLP variables. Also, since $\wp$ is modeled by a Gaussian mixture, the state constraint (18) is always satisfied and needs not be included in the NLP. The solution $\boldsymbol{\zeta}^*$ of the NLP in (34) is obtained using an SQP algorithm that solves the Karush-Kuhn-Tucker (KKT) optimality conditions by representing (34) as a sequence of unconstrained quadratic programming (QP) subproblems with objective function $J_S(\boldsymbol{\zeta}) = J_D(\boldsymbol{\zeta}) + \sum_\jmath \boldsymbol{\lambda}_\jmath \boldsymbol{\xi}_\jmath(\boldsymbol{\zeta})$, where $\boldsymbol{\xi}_\jmath$ denotes the $\jmath$th constraint in (34), and $\boldsymbol{\lambda}_\jmath$ denotes a vector of multipliers of proper dimensions.

At every major iteration ℓ of the SQP algorithm, the Hessian matrix $\mathbf{H} = \partial J_S / \partial \boldsymbol{\zeta}$ is approximated using the Broyden-Fletcher-Goldfarb-Shanno (BFGS) rule

$$\mathbf{H}_{\ell+1} = \mathbf{H}_\ell + \frac{\mathbf{q}_\ell \mathbf{q}_\ell^T}{\mathbf{q}_\ell^T \Delta \boldsymbol{\zeta}_\ell} - \frac{\mathbf{H}_\ell^T \Delta \boldsymbol{\zeta}_\ell^T \Delta \boldsymbol{\zeta}_\ell \mathbf{H}_\ell}{\Delta \boldsymbol{\zeta}_\ell^T \mathbf{H}_\ell \Delta \boldsymbol{\zeta}_\ell} \tag{35}$$

where $\Delta \boldsymbol{\zeta}_\ell = \boldsymbol{\zeta}_\ell - \boldsymbol{\zeta}_{\ell-1}$, and $\mathbf{q}_\ell$ is the change in the gradient $\nabla J_S = \partial J_S / \partial \boldsymbol{\zeta}$ at the ℓth iteration [47]. The Hessian approximation (35) is then used to generate a QP subproblem

$$\begin{aligned}&\min \quad h(\mathbf{d}_\ell) = \left(\frac{1}{2}\right) \mathbf{d}_\ell^T \mathbf{H}_\ell \mathbf{d}_\ell + \nabla J_S^T \mathbf{d}_\ell \\ &\text{sbj to } \nabla \boldsymbol{\xi}_\jmath^T \mathbf{d}_\ell + \boldsymbol{\xi}_\jmath = \mathbf{0}, \forall \jmath\end{aligned} \tag{36}$$

in the search direction $\mathbf{d}_\ell$. The optimal search direction $\mathbf{d}_\ell^*$ is computed from the above QP using an off-the-shelf QP solver [48], such that $\boldsymbol{\zeta}_{\ell+1} = \boldsymbol{\zeta}_\ell + \alpha_\ell \mathbf{d}_\ell^*$.

The step size α_ℓ is determined by an approximate line search in the direction $\mathbf{d}_\ell^*$, aimed at producing a sufficient decrease in the merit function

$$\Psi(\boldsymbol{\zeta}_\ell) = J(\boldsymbol{\zeta}_\ell) + \sum_\jmath \mathbf{r}_{\ell,\jmath}^T \boldsymbol{\xi}_\jmath(\boldsymbol{\zeta}_\ell) \tag{37}$$

TABLE I
COMPUTATIONAL COMPLEXITY OF THE SQP SOLUTION

	DOC	Classical OC
Hessian update	$O(ZXK^2)$	$O(nmN^2K^2)$
QP subproblem	$O(Z^2XK^3)$	$O(nm^2N^3K^3)$
Line search	$O(XK)$	$O(nNK)$

based on the Armijo condition, and a penalty parameter $\mathbf{r}_{\ell,\jmath}$ defined in [47]. The algorithm terminates when the KKT conditions are satisfied within a desired tolerance.

The NLP solution $\boldsymbol{\zeta}^*$ provides the optimal agent PDF $\wp^*$ according to (32), and $\wp^*$ can be used to obtain a microscopic control law $\mathbf{u}_i^*(t_k) = \mathbf{c}[\wp^*(\mathbf{x}_i, t_k)]$ for each sensor using the potential field approach presented in [18]. Other PDF-based control approaches, such as Voronoi diagrams [26], [27], or virtual boundary methods [28] can potentially also be used since the optimal *and* reachable PDF is now known from $\wp^*$.

VII. COMPUTATIONAL COMPLEXITY ANALYSIS

The computational complexity of the direct DOC method presented in the previous section is compared to that of a direct method for classical optimal control (OC) taken from [49]. The direct method in [49] obtains an NLP representation of the classical optimal control problem by discretizing N-coupled ODEs in the form (1) and the corresponding integral cost function about a finite set of collocation points. Subsequently, the NLP solution can be obtained using an SQP algorithm with the computational complexity shown in Table I (Classical OC). This classical direct method was also used in [16] to optimize the track coverage of a mobile sensor network for $N < 100$.

Similar to classical OC, the computational complexity of the SQP algorithm for DOC, described in Section VI, can be analyzed by determining the computation required by the three most expensive steps, namely, the Hessian update (35), the solution of the QP subproblem (36), and the line-search minimization of the merit function (37). As shown in Table I, the solution of the QP subproblem, which is carried out by a QR decomposition of the active constraints using Householder Triangularization [47], is the dominant computation in determining $\wp^*$.

It can be easily shown (Section VIII) that the computation required to obtain the microscopic control law from $\wp^*$ grows linearly with N. Thus, the computation required by the DOC direct method exhibits cubic growth only with respect to K, and quadratic growth with respect to Z. On the other hand, the computation required by the classical OC direct method exhibits cubic growth with respect to K and N, and becomes prohibitive for $N >> 1$. Thus, for sensor networks with $X \ll nN$ and $Z \ll mN$, the DOC approach can bring about considerable computational savings.

VIII. SIMULATION RESULTS

The effectiveness of the DOC approach presented in the previous sections is demonstrated on a network of $N = 250$ omnidirectional sensors that are each installed on a vehicle with nonlinear unicycle kinematics

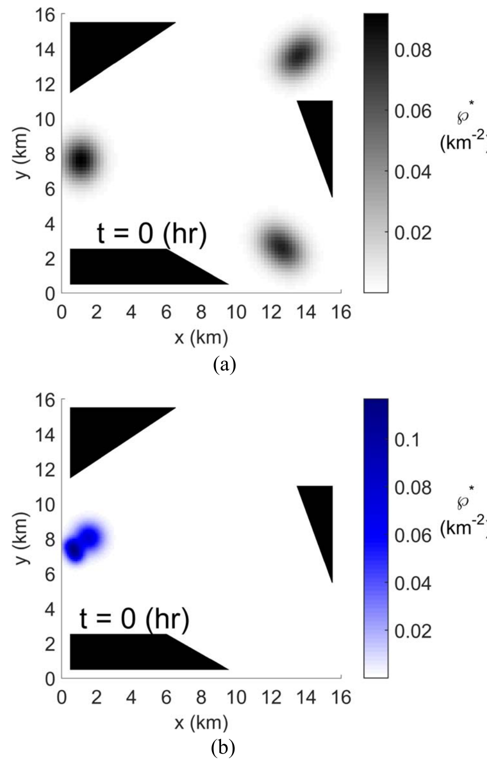

Fig. 2. Initial sensor distribution in (a) and PDF of initial target distribution in (b) in an ROI with three obstacles.

$$\dot{x}_i = v_i \cos\theta_i \quad \dot{y}_i = v_i \sin\theta \quad \dot{\theta}_i = \omega_i \tag{38}$$

and deployed in an obstacle-populated workspace $\mathcal{A} = [0, L] \times [0, L]$ shown in Fig. 2(b), with $L = 16$ km, over a time interval $(T_0, T_f]$, with $T_0 = 0$ and $T_f = 15$ hr. The sensor state $\mathbf{s}_i = [x_i \; y_i \; \theta_i]^T$ consists of the sensor x, y-coordinates, and sensor heading angle θ_i. The sensor control vector is $\mathbf{u}_i = [v_i \; \omega_i]^T$, where v_i is the linear velocity, and ω_i is the angular velocity. The sensors are assumed to have constant linear velocities of $v_i = 0.5$ km/hr, and maximum angular velocities of $\omega_{max} = 0.52$ rad/s, such that $\omega \in [-\omega_{max}, +\omega_{max}]$. It is assumed that the sensors are deployed in $\mathcal{A}$ with an initial distribution $\wp_0$ [Fig. 2(a)] and, thus, at $t = T_0$ they are located at a set of initial positions sampled from $\wp_0$. The number of independent elementary detections required to declare a target track detection is chosen to be $k = 3$, and the sensor effective range is $r = 0.2$ km.

The PDF of the initial target position ($j = 0$) is plotted in Fig. 2(b), and is modeled by the Gaussian mixture

$$f(\mathbf{x}_{T_0}) = \sum_{\ell=1}^{3} \frac{w_\ell}{(2\pi)^{\frac{n}{2}} \det(\boldsymbol{\Sigma}_\ell)^{\frac{1}{2}}} e^{\left[-\left(\frac{1}{2}\right)(\mathbf{x}_{T_0} - \boldsymbol{\mu}_\ell)^T \boldsymbol{\Sigma}_\ell^{-1} (\mathbf{x}_{T_0} - \boldsymbol{\mu}_\ell)\right]} \tag{39}$$

where $\boldsymbol{\mu}_1 = [0.5 \quad 7.5]^T$ km, $\boldsymbol{\mu}_2 = [0.75 \quad 7]^T$ km, and $\boldsymbol{\mu}_3 = [1.5 \quad 8]^T$ km, and $\boldsymbol{\Sigma}_1 = 0.1\,\mathbf{I}_2$, $\boldsymbol{\Sigma}_2 = 0.1\,\mathbf{I}_2$, and $\boldsymbol{\Sigma}_3 = .3\,\mathbf{I}_2$. The mixing proportions are $w_1 = 0.2$, $w_2 = 0.2$, and $w_3 = 0.6$. The Markov model PDFs are shown in Table II, and the

TABLE II
MARKOV MOTION MODEL PROBABILITY DENSITY FUNCTIONS (PDFS)

Sub-interval, $(t_j,\ t_{j+1}]$ **(hr)**	**Heading PDF,** $f_{\Theta_{T_j}}(\theta_{T_j})$	**Velocity PDF,** $f_{V_{T_j}}(v_{T_j})$
$j=1$: (0, 5] (hr)	$\mathcal{N}(\mu,\sigma)$, $\mu=2\pi/9$, $\sigma=\pi/24$	$\mathcal{U}(\mathcal{V})$, $\mathcal{V}=[.9,\ .925]$
$j=2$: (5, 10] (hr)	$\mathcal{N}(\mu,\sigma)$, $\mu=-\pi/6$, $\sigma=\pi/24$	$\mathcal{N}(\mu,\sigma)$, $\mu=.8$, $\sigma=0.025$
$j=3$: (10, 15] (hr)	$\text{Mult}_2(w_i;\mu_i,\sigma_i)$, $w_1=0.5$, $\mu_1=-\pi/3$, $\sigma_1=\pi/32$, $w_2=0.5$, $\mu_2=\pi/3$, $\sigma_2=\pi/32$	$\mathcal{U}(\mathcal{V})$, $\mathcal{V}=[1.2,\ 1.25]$

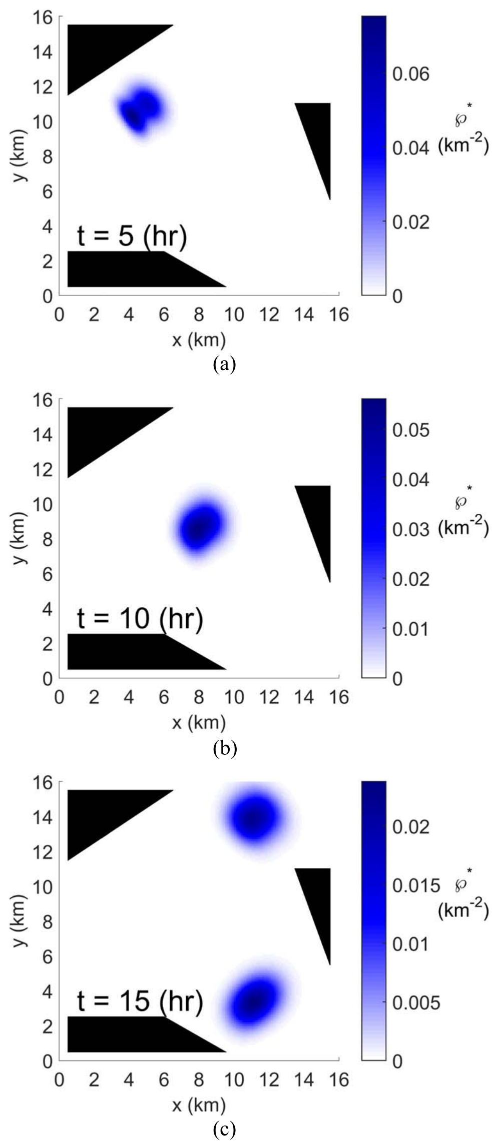

Fig. 3. Evolution of target PDF at three instants in time.

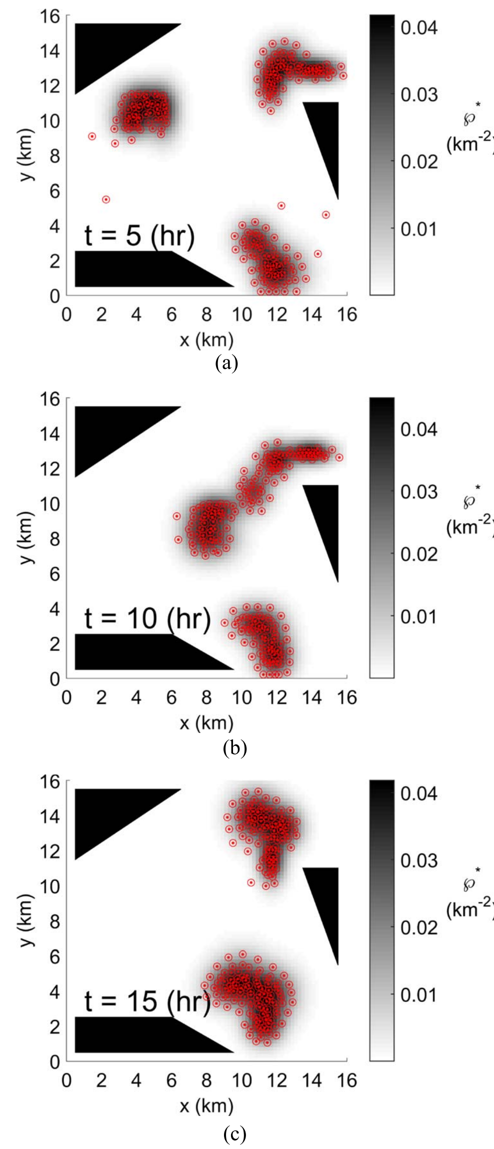

Fig. 4. Evolution of optimal sensor PDF $\wp^*$ microscopic state (red dots) and FOVs (red circles) at three instants in time.

evolution of the target PDF over time obtained by numerical integration is plotted in Fig. 3. The cost function weights are chosen to be $w_s = 1$, $w_r = 0.02$, and $w_e = 0.1$, based on the relative importance of the sensing, obstacle-avoidance, and energy objectives, respectively.

The optimal time-varying PDF $\wp^*$ is obtained using the direct DOC method presented in Section VI, where the chosen number of mixture components is $Z = 9$, the state space is discretized into $X = 900$ collocation points, for $\Delta t = 1$ hr, and $K = 15$. Given $\wp^*$ and the estimated sensor PDF $\hat{\wp}$, an attractive potential

$$U(\mathbf{x}_i, t_k) \triangleq \frac{1}{2}\left[\hat{\wp}(\mathbf{x}_i, t_k + \delta t) - \wp^*(\mathbf{x}_i, t_k + \delta t)\right]^2 \qquad (40)$$

can be used to generate virtual forces that pull the sensors toward $\wp^*$ for a small time increment δt [18]. At any time t_k, the sensor PDF can be estimated efficiently from measurements

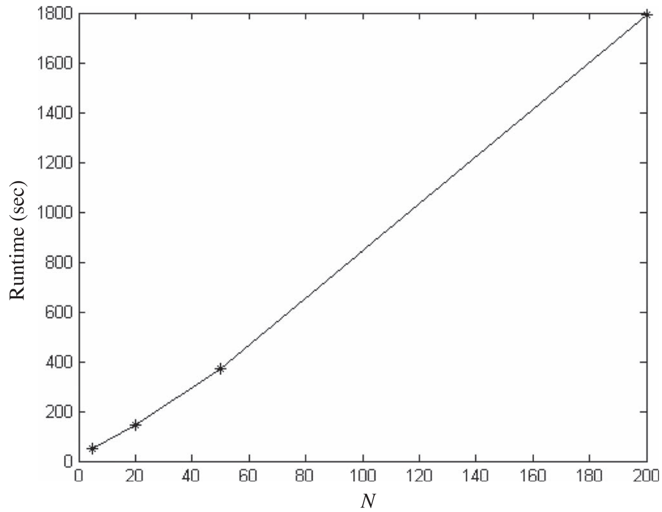

Fig. 5. Time required to compute the microscopic control law in (41) as a function of the number of sensors.

of the microscopic sensor state using Kernel density estimation [19]. Then, the microscopic feedback control law

$$\mathbf{u}_i^*(t_k) = [v_i \;\; Q(\theta_i, \phi)]^T \tag{41}$$

can be shown to minimize (40) and provide closed-loop stability, provided $\phi = -\nabla U(\mathbf{x}_i, t_k)$ and

$$Q(\cdot) \triangleq \{\vartheta(\theta_i) - \vartheta[\Theta(\phi)]\} \,\mathrm{sgn}\, \{\vartheta[\Theta(\phi)] - \vartheta(\theta)\} \tag{42}$$

represents the minimum differential between the actual heading angle θ_i and the desired heading angle $\Theta(\phi)$ computed from the gradient of the attractive potential function (40), where sgn$(\cdot)$ is the sign function, and $\vartheta(\cdot)$ is an angle wrapping function [39].

The optimal sensor PDF and microscopic sensor state and FOVs obtained by DOC are plotted in Fig. 4, at three sample moments in time. The probabilities of detection of these four methods are presented in Fig. 9. From these simulations, it can be seen that the sensors are maximizing the probability of detection by anticipating the target motion forecast, while also avoiding obstacles and minimizing energy consumption. As shown in Fig. 5, $\wp^*$ can be used to generate control laws with a cost linear in the number of sensors N.

The performance of the DOC method is compared to four existing sensor network deployment strategies known as stochastic gradient, uniform, grid, and random strategies. Uniform, grid, and random strategies are static deployments in which N sensor positions are obtained using finite-mixture sampling [33]. The uniform deployment is obtained by sampling a uniform distribution over the obstacle-free space in $\mathcal{A}$. The grid deployment is obtained by sampling a Gaussian mixture with $Z = 11$ components centered on a grid, and the random deployment samples a Gaussian mixture with $Z = 15$ components randomly centered in $\mathcal{A}$. In these static deployment strategies, collisions can be avoided by removing components that overlap obstacles, and by requiring sampled positions to be at a desired minimum distance from the nearest obstacle, as shown by the deployment examples in Fig. 6.

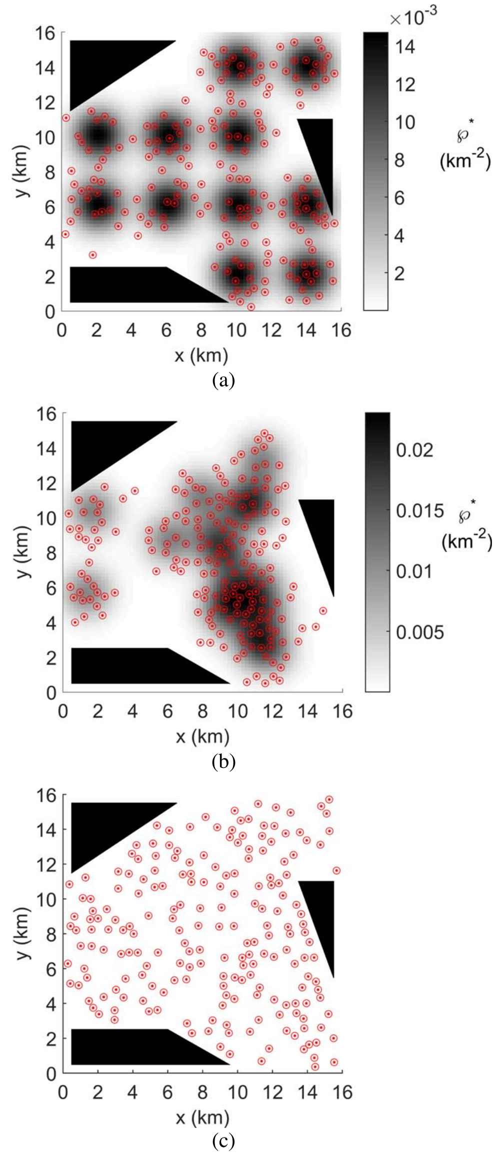

Fig. 6. (a) Grid, (b) random, and (c) uniform sensor deployments (black dots) and corresponding FOVs (black circles).

The stochastic gradient method presented in [34] is also simulated here for comparison. This method obtains the control law for each sensor from the gradient of a function of the sensor initial and goal state in $\mathcal{A}$. Uncertainties in the state measurements or environmental dynamics result in the control law that is obtained from the stochastic gradient descent of an appropriately chosen function. For the example in Fig. 2(b), the initial sensor states are sampled from $\wp_0$, and the goal states are sampled from a time-invariant goal sensor PDF that minimizes the cost function (14) at T_f, and is plotted in Fig. 7. With this approach, each sensor seeks to move toward the closest goal state not occupied by another sensor, and avoids obstacles by means of a repulsive potential term, denoted by U_{rep}. Then, a feedback control law for sensors i, described by the unicycle kinematics in (38), can be obtained in the form (41) by letting $U = w_a\|\mathbf{x}_i^* - \mathbf{x}_{i_0}\| + w_b U_{rep}$, where $\mathbf{x}_i^*$ is the goal state, $\mathbf{x}_{i_0}$ is the initial state, and $w_a = 1$ and $w_b = 2.5$ are weighting constants.

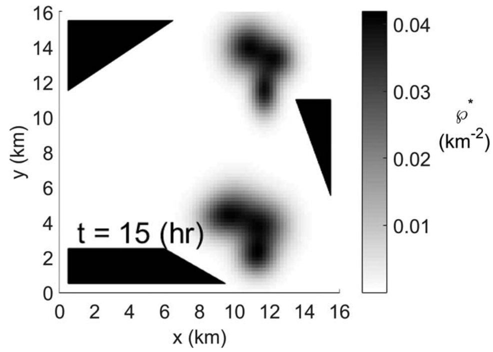

Fig. 7. Goal sensor PDF for the stochastic gradient method.

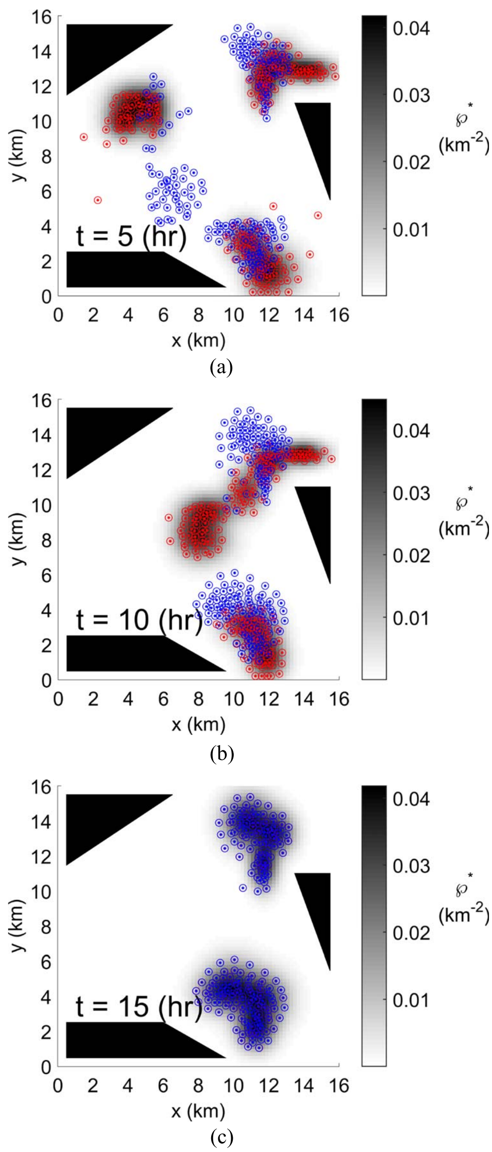

Fig. 8. Comparison between stochastic gradient sensor positions (blue dots) with corresponding FOVs (blue circles), and DOC sensor positions and FOVs (red dots and circles).

The results obtained by the stochastic gradient method are plotted in Fig. 8 at three sample moments in time. It can be seen that at the final time [Fig. 8(c)], the sensors have reached the goal states sampled from the distribution in Fig. 7 known to maximize the probability of detection at T_f. As a result, the final sensor positions in Fig. 8(c) are very close to the final sensor positions obtained by DOC. But while the stochastic gradient approach provides optimal performance only at T_f, the DOC approach optimizes performance over the entire time interval $(T_0,\ T_f]$, as shown in Fig. 5.

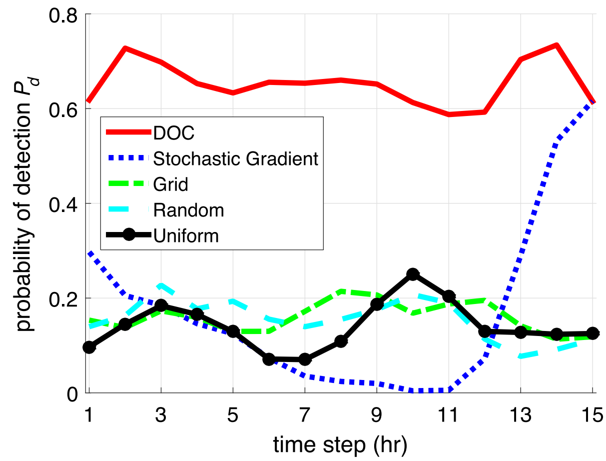

Fig. 9. Comparison of probability of detection.

For each deployment strategy, the sensor performance is assessed by evaluating and averaging the actual number of target track detections obtained by 20 simulated sensor networks. The cost function (14) is also evaluated by estimating the sensor PDF from the microscopic sensor states using kernel density estimation with a standard Gaussian kernel at every time step in $(T_0,\ T_f]$. The performance comparison results, summarized in Fig. 5, show that the DOC method significantly outperforms all other strategies by providing a probability of detection that is up to three times as large as the peak performance by other methods. These results are representative of a number of simulations involving different sensor initial conditions and different target PDFs.

IX. Conclusion

This paper presents a DOC approach for controlling a network of mobile omnidirectional sensors deployed to cooperatively track and detect moving targets in a region of interest. Several authors have shown that the performance of cooperative multiagent networks, such as sensor networks, can, in many cases, be represented as a function of the agent PDF. Existing approaches, however, assume that the optimal or goal PDF is known *a priori*. This paper shows that the DOC approach can be used to optimize a time-varying agent PDF subject to the agent dynamic or kinematic equations. This paper also shows that since the closed-loop DOC problem has a Hamiltonian structure, an efficient direct method of solution can be obtained using a finite-volume discretization scheme that has a computational complexity far reduced compared to that of classical OC. The numerical simulation results show that the direct DOC method presented in this paper is applicable to networks with hundreds of sensors and, as a result, the network performance can be significantly increased compared to existing stochastic gradient, uniform, grid, and random deployment strategies.

REFERENCES

[1] H. Choset, "Coverage for robotics: A survey of recent results," *Ann. Math. Artif. Intell.*, vol. 31, no. 1–4, pp. 113–126, 2001.

[2] T. Clouqueur, V. Phipatanasuphorn, P. Ramanathan, and K. Saluja, "Sensor deployment for detection of targets traversing a region," *Mobile Netw. Appl.*, vol. 8, pp. 453–461, Aug. 2003.

[3] K. Chakrabarty, S. S. Iyengar, H. Qi, and E. Cho, "Grid coverage for surveillance and target location in distributed sensor networks," *IEEE Trans. Comput.*, vol. 51, no. 12, pp. 1448–1453, 2002.

[4] K. C. Baumgartner, S. Ferrari, and T. Wettergren, "Robust deployment of dynamic sensor networks for cooperative track detection," *IEEE Sens.*, vol. 9, no. 9, pp. 1029–1048, 2009.

[5] K. C. Baumgartner and S. Ferrari, "A geometric transversal approach to analyzing track coverage in sensor networks," *IEEE Trans. Comput.*, vol. 57, no. 8, pp. 1113–1128, 2008.

[6] K. A. C. Baumgartner and S. Ferrari, "Optimal placement of a moving sensor network for track coverage," in *Proc. Amer. Controls Conf.*, New York, USA, Jul. 2007, pp. 4040–4046.

[7] S. Ferrari, R. Fierro, and D. Tolic, "A geometric optimization approach to tracking maneuvering targets using a heterogeneous mobile sensor network," *Proc. IEEE Conf. Decis. Control*, Shanghai, China, 2009.

[8] K. A. C. Baumgartner, S. Ferrari, and A. V. Rao, "Optimal control of a mobile sensor network for cooperative target detection," *IEEE J. Ocean. Eng.*, vol. 34, no. 4, pp. 678–697, 2009.

[9] B. Bernard and S. Ferrari, "A geometric transversals approach to track coverage of maneuvering targets," *Proc. IEEE Conf. Dec. Control*, Atlanta, GA, USA, pp. 1243–1249, 2010.

[10] H. Wei and S. Ferrari, "A geometric transversals approach to analyzing the probability of track detection for maneuvering targets," *IEEE Trans. Comput.*, vol. 63, no. 11, pp. 2633–2646, 2014.

[11] S. Ferrari and G. Daugherty, "A q-learning approach to automated unmanned air vehicle demining," *J. Defense Model. Simul.*, vol. 9, pp. 83–92, 2011.

[12] G. Zhang and S. F. M. Qian, "Information roadmap method for robotic sensor path planning," *J. Intell. Robot. Syst.*, vol. 56, pp. 69–98, 2009.

[13] S. Ferrari, R. Fierro, B. Perteet, C. Cai, and K. Baumgartner, "A geometric optimization approach to detecting and intercepting dynamic targets using a mobile sensor network," *SIAM J. Control Optimiz.*, vol. 48, no. 1, pp. 292–320, 2009.

[14] C. Cai and S. Ferrari, "Information-driven sensor path planning by approximate cell decomposition," *IEEE Trans. Syst., Man, Cybern. B, Cybern.*, vol. 39, no. 2, 2009.

[15] C. Cai and S. Ferrari, "Comparison of information-theoretic objective functions for decision support in sensor systems," in *Proc. Amer. Control Conf.*, New York, USA, 2007, pp. 63–133.

[16] K. C. Baumgartner, S. Ferrari, and A. Rao, "Optimal control of an underwater sensor network for cooperative target tracking," *IEEE J. Ocean. Eng.*, vol. 34, no. 4, pp. 678–697, 2009.

[17] K. Rudd, G. Foderaro, and S. Ferrari, "A generalized reduced gradient method for the optimal control of multiscale dynamical systems," in *Proc. IEEE Conf. Dec. Control*, Florence, Italy, 2013.

[18] G. Foderaro, S. Ferrari, and T. Wettergren, "Distributed optimal control for multi-agent trajectory optimization," *Automatica*, vol. 50, pp. 149–154, 2014.

[19] G. Foderaro, S. Ferrari, and M. Zavlanos, "A decentralized kernel density estimation approach to distributed robot path planning," in *Proc. Neural Inf. Process. Syst. Conf.*, Lake Tahoe, NV, USA, 2012.

[20] G. Foderaro and S. Ferrari, "Necessary conditions for optimality for a distributed optimal control problem," *Proc. IEEE Conf. Dec. Control*, Atlanta, GA, USA, pp. 4831–4838, 2010.

[21] S. Ferrari, G. Zhang, and T. Wettergren, "Probabilistic track coverage in cooperative sensor networks," *IEEE Trans. Syst., Man, Cybern. B, Cybern.*, vol. 40, no. 6, 2010.

[22] S. Berman, A. Halasz, M. Hsieh, and V. Kumar, "Navigation-based optimization of stochastic strategies for allocating a robot swarm among multiple sites," *Proc. Dec. Control Conf.*, pp. 4376–4381, 2008.

[23] J. Oyekan and H. Hu, "Ant robotic swarm for visualizing invisible hazardous substances," *Robotics*, vol. 2, pp. 1–18, 2013.

[24] S. Berman, A. Halasz, M. Hsieh, and V. Kumar, "Optimized stochastic policies for task allocation in swarms of robots," *IEEE Trans. Robot.*, vol. 25, no. 4, pp. 927–937, 2009.

[25] T. Wettergren and R. Costa, "Optimal placement of distributed sensors against moving targets," *ACM Trans. Sens. Netw.*, vol. 5, no. 3, 2009.

[26] J. Cortes, C. Martinez, T. Karatas, and F. Bullo, "Coverage control for mobile sensing networks," *IEEE Trans. Robot. Autom.*, vol. 20, no. 2, pp. 243–255, 2004.

[27] S. Martinez, J. Cortes, and F. Bullo, "Motion coordination with distributed information," *IEEE Control Syst. Mag.*, vol. 27, no. 4, pp. 75–88, 2007.

[28] N. Ayanian and V. Kumar, "Abstractions and controllers for groups of robots in environments with obstacles," *Proc. IEEE Int. Conf. Robot. Autom.*, Anchorage, AK, USA, 2010.

[29] H. Wei and S. Ferrari, "A geometric transversals approach to sensor motion planning for tracking maneuvering targets," *IEEE Trans. Autom. Control*, vol. 60, no. 10, pp. 2773–2778, Oct. 2015.

[30] T. A. Wettergren, "Performance of search via track-before-detect for distributed sensor networks," *IEEE Trans. Aerosp. Electron. Syst.*, vol. 44, no. 1, pp. 314–325, Jan. 2008.

[31] T. A. Wettergren, R. L. Streit, and J. R. Short, "Tracking with distributed sets of proximity sensors using geometric invariants," *IEEE Trans. Aerosp. Electron. Syst.*, vol. 40, no. 4, pp. 1366–1374, Oct. 2004.

[32] R. Costa and T. A. Wettergren, "Assessing design tradeoffs in deploying undersea distributed sensor networks," in *Proc. OCEANS*, Vancouver, BC, Canada, Sep. 2007, pp. 1–5.

[33] G. McLachlan, *Finite Mixture Models*. New York, USA: Wiley, 2000.

[34] J. L. Ny and G. J. Pappas, "Sensor-based robot deployment algorithms," *Proc. IEEE Conf. Dec. Control*, pp. 5486–5492, 2010.

[35] S. B. Pope, *Turbulent Flows*. Cambridge, U.K.: Cambridge University Press, 2000.

[36] Y. Bar-Shalom, X. Li, and T. Kirubarajan, *Estimation with Applications to Tracking and Navigation: Algorithms and Software for Information Extraction*. Hoboken, NJ, USA: Wiley, 2001.

[37] Y. Bar-Shalom and X.-R. Li, *Estimation and Tracking: Principles, Techniques, and Software*. Norwood, MA, USA: Artech House, 1993, vol. 393.

[38] Y. Bar-Shalom and E. W. D. Blair, *Multitarget-Multisensor Tracking: Applications and Advances*, Vol. III. Boston, MA, USA: Artech House, 2000.

[39] J. C. Latombe, *Robot Motion Planning*. Norwood, MA, USA: Kluwer, 1991.

[40] J. P. Boyd, *Chebyshev and Fourier Spectral Methods*, II Ed. New York, USA: Dover, 2001.

[41] J. C. Tannehille, D. A. Anderson, and R. H. Pletcher, *Computational Fluid Mechanics and Heat Transfer*. New York, USA: Taylor & Francis, 1997.

[42] I. M. Gelfand and S. V. Fomin, *Calculus of Variations*. Englewood Cliffs, NJ, USA: Prentice-Hall, 1963.

[43] D. E. Kirk, *Optimal Control Theory: An Introduction*. Englewood Cliffs, NJ, USA: Prentice-Hall, 1970.

[44] M. F. M. Speetjens, "Topology of advective-diffusive scalar transport in laminar flows," *Phys. Rev. E*, vol. 77, no. 2, 2008.

[45] K. Bajer, "Hamiltonian formulation of the equations of streamlines in three-dimensional steady flows," *Chaos, Solitons Fractals*, vol. 4, no. 6, pp. 895–911, 1994.

[46] S. Ferrari, G. Foderaro, P. Zhu, and T. A. Wettergren, "Distributed optimal control of multiscale dynamical systems: A tutorial," *IEEE Control Syst. Mag.*, vol. 36, no. 2, pp. 102–116, 2016.

[47] M. J. D. Powell, "A fast algorithm for nonlinearly constrained optimization calculations," *Numer. Anal.*, vol. 630, 1978.

[48] Mathworks, Matlab Optimization Toolbox. [Online]. Avaliable: http://www.mathworks.com, 2004, *Function: Fmincon*.

[49] J. Betts, "Survey of Numerical Methods for Trajectory Optimization," *J. Guidance, Control, Dynam.*, vol. 21, no. 2, pp. 193–207, 1998.

Greg Foderaro (M'13) received the B.S. degree in mechanical engineering from Clemson University, Clemson, SC, USA, in 2009 and the Ph.D. degree in mechanical engineering and materials science from Duke University, Durham, NC, USA, in 2013.

Currently, he is a Staff Engineer with Applied Research Associates, Inc. His research interests are in underwater sensor networks, robot path planning, multiscale dynamical systems, pursuit-evasion games, and spiking neural networks.

Pingping Zhu (M'17) received the B.S. degree in electronics and information engineering and the M.S. degree in pattern recognition and artificial intelligence from Huazhong University of Science and Technology, and the M.S. and Ph.D. degrees in electrical and computer engineering from the University of Florida, Gainesville, FL, USA.

Currently, he is a Research Associate with the Department of Mechanical and Aerospace Engineering with Cornell University, Ithaca, NY, USA. Previously, he was a Postdoctoral Associate with the Department of Mechanical Engineering and Material Science at Duke University, Durham, NC, USA. His research interests include approximate dynamic programming, optimal control of mobile sensor networks, signal processing, machine learning, and neural networks.

Hongchuan Wei received the B.S. degree in vehicle engineering from Tsinghua University, Beijing, China, in 2010 and is currently pursuing the Ph.D. degree at Duke University, Durham, NC, USA.

The probability of detection is a function of the target movement and sensors field of view. He is also interested in utilizing information-theoretic functions to acquire optimal sensor controls in order to learn the behaviors of targets described by non-parametric Bayesian models. His research interest includes sensor network deployment, which consists of optimally placing a set of sensors in a region of interest (ROI) such that the probability of detection of targets traveling through the ROI is maximized.

Thomas A. Wettergren (SM'06) received the B.S. degree in electrical engineering and the Ph.D. degree in applied mathematics from Rensselaer Polytechnic Institute, Troy, NY, USA.

He joined the Naval Undersea Warfare Center, Newport, RI, USA, in 1995, where he has served as a Research Scientist in the torpedo systems, sonar systems, and undersea combat systems departments. He currently serves as the US Navy Senior Technologist (ST) for Operational and Information Science, with a concurrent title as a Senior Research Scientist at the Center. He also is an Adjunct Professor of Mechanical Engineering at Pennsylvania State University, University Park, PA, USA. His personal research interests are in planning and control of distributed systems, applied optimization, multiagent systems, and search theory.

Dr. Wettergren is a member of the Society for Industrial and Applied Mathematics.

Silvia Ferrari (SM'13) received the B.S. degree from Embry-Riddle Aeronautical University, Daytona Beach, FL, USA, and the M.A. and Ph.D. degrees from Princeton University, Princeton, NJ, USA.

Currently, she is a Professor of Mechanical and Aerospace Engineering at Cornell University, Ithaca, NY, USA. Previously, she was Professor of Engineering and Computer Science, and Founder and Director of the NSF Integrative Graduate Education and Research Traineeship (IGERT) and Fellowship program on Wireless Intelligent Sensor Networks (WISeNet) at Duke University, Durham, NC, USA. She is the Director of the Laboratory for Intelligent Systems and Controls (LISC), and her principal research interests include robust adaptive control of aircraft, learning and approximate dynamic programming, and optimal control of mobile sensor networks.

Prof. Ferrari is a member of ASME, SPIE, and AIAA. She is the recipient of the ONR young investigator award (2004), the National Science Foundation CAREER award (2005), and the Presidential Early Career Award for Scientists and Engineers (PECASE) award (2006).